ACS Chemical Neuroscience
Cite This: ACS Chem. Neurosci. 2018, 9, 1128−1140
Research Article
pubs.acs.org/chemneuro

What Contributes to Serotonin−Norepinephrine Reuptake Inhibitors' Dual-Targeting Mechanism? The Key Role of Transmembrane Domain 6 in Human Serotonin and Norepinephrine Transporters Revealed by Molecular Dynamics Simulation

Weiwei Xue,[†,§] Fengyuan Yang,[†,§] Panpan Wang,[†,§] Guoxun Zheng,[†,§] Yuzong Chen,[‡] Xiaojun Yao,[∥] and Feng Zhu*[,†,§]

[†]Innovative Drug Research and Bioinformatics Group, College of Pharmaceutical Sciences, Zhejiang University, Hangzhou 310058, China

[§]Innovative Drug Research and Bioinformatics Group, School of Pharmaceutical Sciences and Collaborative Innovation Center for Brain Science, Chongqing University, Chongqing 401331, China

[‡]Bioinformatics and Drug Design Group, Department of Pharmacy, National University of Singapore, Singapore 117543, Singapore

[∥]State Key Laboratory of Applied Organic Chemistry and Department of Chemistry, Lanzhou University, Lanzhou 730000, China

Supporting Information

ABSTRACT: Dual inhibition of serotonin and norepinephrine transporters (hSERT and hNET) gives greatly improved efficacy and tolerability for treating major depressive disorder (MDD) compared with selective reuptake inhibitors. Pioneer studies provided valuable information on structure, function, and pharmacology of drugs targeting both hSERT and hNET (serotonin−norepinephrine reuptake inhibitors, SNRIs), and the differential binding mechanism between SNRIs and selective inhibitors of 5-HT (SSRIs) or NE (sNRIs) to their corresponding targets was expected to be able to facilitate the discovery of a privileged drug-like scaffold with improved efficacy. However, the dual-target mechanism of SNRIs was still elusive, and the binding mode distinguishing SNRIs from SSRIs and sNRIs was also unclear. Herein, an integrated computational strategy was adopted to discover the binding mode shared by all FDA approved SNRIs. The comparative analysis of binding free energy at the per-residue level discovered that residues Phe335, Leu337, Gly338, and Val343 located at the transmembrane domain 6 (TM6) of hSERT (the corresponding residues Phe317, Leu319, Gly320, and Val325 in hNET) were the determinants accounting for SNRIs' dual-acting inhibition, while residues lining TM3 and 8 (Ile172, Ser438, Thr439, and Leu443 in hSERT; Val148, Ser419, Ser420, and Met424 in hNET) contributed less to the binding of SNRIs than that of SSRIs and sNRIs. Based on these results, the distances between an SNRI's centroid and the centroids of its two aromatic rings (measuring the depth of rings stretching into hydrophobic pockets) were discovered as the key to the SNRIs' dual-targeting mechanism. This finding revealed SNRIs' binding mechanism at an atomistic level, which could be further utilized as structural blueprints for the rational design of privileged drug-like scaffolds treating MDD.

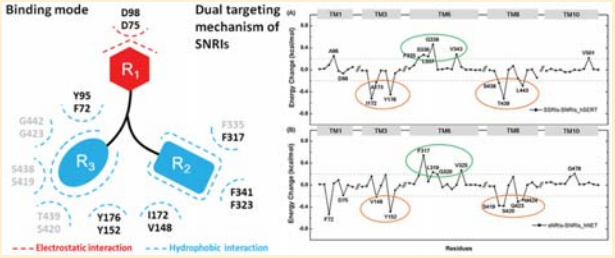

KEYWORDS: *Serotonin−norepinephrine reuptake inhibitor, major depressive disorder, dual-target drug, binding mode, molecular dynamics*

INTRODUCTION

Major depressive disorder (MDD) has been estimated as the second largest global burden among all diseases by 2030,[1,2] which makes the discovery of novel and efficacious antidepressants in urgent need.[3,4] The development of MDD is discovered to be closely related to the deficiency of two neurotransmitters in brain: serotonin (5-HT) and norepinephrine (NE),[5] the corresponding transporters (hSERT and hNET) of which play critical roles in regulating the duration and intensity of the neurotransmitter signal in the synaptic cleft.[6−10] In light of these, selective 5-HT reuptake inhibitors (SSRIs) and selective NE reuptake inhibitors (sNRIs) are approved by the U.S. Food and Drug Administration (FDA) and recognized as a milestone in MDD treatment.[11,12] However, their side effects, delayed onset of action, and partial or no response for some patients limit their efficacy and patient tolerance and thus severely hamper their prescription usage.[13,14] Recently, a novel class of antidepressants simultaneously inhibiting hSERT and hNET (serotonin−norepinephrine reuptake inhibitors, SNRIs) was discovered.[11] Because of their capability of sustaining the

Received: December 7, 2017
Accepted: January 4, 2018
Published: January 4, 2018

DOI: 10.1021/acschemneuro.7b00490
ACS Chem. Neurosci. 2018, 9, 1128−1140

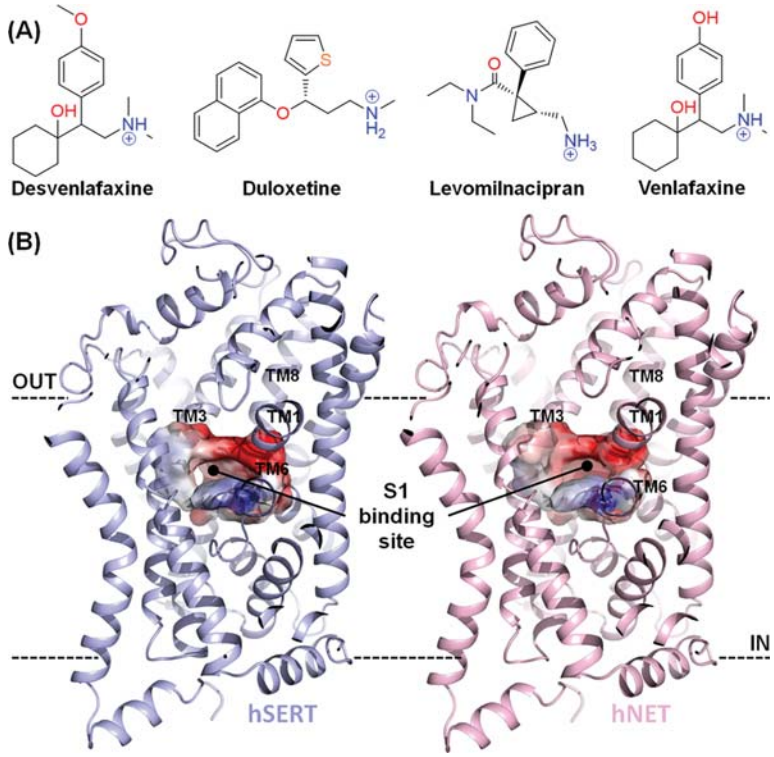

Figure 1. Drugs and protein targets studied in this work. (A) Chemical structures of four currently marketed SNRI antidepressants approved by U.S. FDA. (B) Homology models of hSERT and hNET. The S1 binding sites primarily surrounded by TM1, TM3, TM6, and TM8 for both hSERT and hNET are highlighted.

level of both 5-HT and NE, SNRIs are reported to give greatly improved efficacy and tolerability compared with selective 5-HT or NE reuptake inhibitors.[15]

Although considerable effort has been made,[16−18] only a few SNRIs with clinical importance for treating MDD were discovered, which included 4 drugs (desvenlafaxine, duloxetine, levomilnacipran, and venlafaxine) approved by the U.S. FDA (Figure 1A).[19−21] The discovery of novel privileged drug-like SNRI scaffolds was reported to be severely limited due to the lack of binding mode information between clinically important SNRIs and their targets.[22,23] To cope with this limitation, X-ray crystal structures of hSERT and hNET homologues, such as bacterial leucine transporter (LeuT),[24] LeuBAT (a LeuT variant engineered to harbor hSERT-like pharmacology by mutating key residues around the primary binding pocket S1)[25] and the *Drosophila melanogaster* dopamine transporter (dDAT),[25] were solved and in turn facilitated drug discovery.[26−28] Meanwhile, site-directed mutagenesis studies on hSERT and hNET identified a variety of residues within the S1 drug-binding site at which mutations influenced the drugs' affinity.[29−31] Besides these experimental endeavors, various computational methods were frequently used to elucidate ligand binding modes in hSERT or hNET,[32−34] and SSRIs binding modes in hSERT were explored and compared with the recently resolved X-ray structure of hSERT at the atomistic scale.[33,35−37] These pioneer studies gave valuable information on the structure, function, and pharmacology of hSERT and hNET.[22] In spite of this progress, cocrystallized structures of clinically important antidepressants (SNRIs, SSRIs, and sNRIs) in complex with their corresponding monoamine transporters, especially the human structures, are still limited, and important mechanistic principles of these antidepressants against targets need to be further explored at the molecular level. An example is the SNRI binding mode and the structural determinants of transporters responsible for drug selectivity, which is the central concern in drug discovery since it substantially influences the efficacy and tolerability of drug candidates. Thus, the understanding of the differential binding mechanism between SNRIs and selective reuptake inhibitors to their corresponding targets was expected to give insight into the discovery of privileged drug-like scaffolds with improved efficacy and patient tolerance.[29,38−41]

However, the mechanism underlying the SNRI dual-target binding mode in both hSERT and hNET was still elusive, and the binding mode distinguishing SNRIs (especially the FDA approved ones) from SSRIs and sNRIs was also unclear.[29,39] Thus, an integrated computational strategy was adopted in this study to discover the binding mode of four FDA approved SNRIs in their targets and reveal key binding mechanisms differentiating SNRIs from SSRIs and sNRIs. In particular, a recently reported template of dDAT[25] with high sequence identity to both hSERT and hNET was first adopted to generate the homology models of these two targets. Then, all FDA approved SNRIs were docked into the modeled targets and used as initial conformations for molecular dynamics (MD) simulation followed by endpoint binding free energy calculation. As a result, a binding mode shared by all those studied SNRIs of various scaffolds was identified through protein−ligand interactions and the clustering analysis of per-residue binding energies, and key physicochemical properties and binding mechanisms differentiating the approved SNRIs from SSRIs and sNRIs were characterized based on their

DOI: 10.1021/acschemneuro.7b00490
ACS Chem. Neurosci. 2018, 9, 1128−1140

Table 1. Comparison of Homology Models (hSERT and hNET) and Crystal Structures (hSERT and dDAT)

	hSERT (dDAT)[a]				hNET (dDAT)[a]			
	whole structure[b]		S1 site (TM1, 3, 6, 8, and 10)[c]		whole structure		S1 site (TM1, 3, 6, 8, and 10)	
	identity (%)	RMSD[d]	identity (%)	RMSD[d]	identity (%)	RMSD[d]	identity (%)	RMSD[d]
hSERT (crystal structure)[b]		2.45		0.80	54		62	
hNET (hSERT)[c]	54		62			4.44		0.81
dDAT (crystal structure)[d,e]	56		67		61		76	

[a]Homology model of hSERT and hNET based on the dDAT crystal structure[25] as a template. [b]Crystal structure of hSERT.[35] [c]Homology model of hSERT and hNET based on the hSERT crystal structure[35] as a template. [d]The whole and S1 site RMSD between homology models and crystal structures were calculated based on protein backbone atoms. [e]Crystal structure of dDAT.[25]

structural and energetic information. In sum, this study drew a blueprint for assessing and discovering novel, safer, and more effective dual-targeting drug scaffolds for not only MDD but also other psychiatric disorders.

RESULTS AND DISCUSSION

Modeled Structures of hSERT and hNET. Homology models of hSERT and hNET were constructed using the high-resolution (2.8 Å) X-ray crystal structure of dDAT (PDB code 4M48,[25] from Glu26 to Asp599) as a template. As the best template so far for monoamine transporter modeling,[22] the dDAT gave a higher degree of sequence identity with hSERT (56%) and hNET (61%) compared with other templates (SI, Figure S1). The constructed homology models of hSERT (from Glu78 to Pro617) and hNET (from Gln54 to Glu597) covered all 7 transmembrane (TM) regions and the corresponding intervening loop (Figure 1B). The stereochemical quality and accuracy of the predicted models was evaluated (SI, Figure S2). As illustrated, 99.6% and 99.8% of the modeled residues of hSERT and hNET were in the "allowed region", which indicated that the overall conformations of the main chain and the side chains were reasonable.

It is important to point out that the X-ray structure of hSERT was solved[35] at the end of this work. Thus, the comparison of hSERT's homology model with its crystal structure was conducted and summarized in Table 1. Although a relatively large root-mean-square deviation (RMSD = 2.45 Å) between the homology model and the crystal structure of hSERT was observed, Figure S3A in SI, their S1 binding sites (surrounded by TM1, 3, 6, 8, and 10) were very similar with RMSD of 0.80 Å (SI, Figure S3B). In addition, the calculated RMSD of the transmembrane domain was 1.33 Å, indicating that large RMSD values were the case for the intervening loops of the membrane protein. Further structural alignment between hSERT's homology model and its crystal structure revealed that the relatively large RMSD mainly originated from their EL2 domains (SI, Figure S3A). In the meantime, hNET's homology model was constructed using hSERT's X-ray crystal structure (PDB code 5I6Z)[35] as a template. Sequence identities between hNET and hSERT for whole protein and for S1 site only were 54% and 62%, respectively, which were lower than those between hNET and dDAT (61% and 76%, shown in Table 1). Superposition between the two hNET homology models is shown in SI, Figure S4. The RMSDs for whole protein, transmembrane domain, and S1 site are 4.44, 1.34 and 0.81 Å, respectively. Taken together, the crystal structure of dDAT[25] did provide an ideal template to construct the homology models of hSERT and hNET, especially of the S1 drug binding site.

Initial Poses of SNRIs Binding to hSERT and hNET. Docking was carried out to determine the initial poses of four SNRIs binding in the homology models of hSERT and hNET. The docking poses oriented in a similar way as SSRIs and SNRIs in LeuBAT[42] were selected for MD simulation and thermodynamic analysis, which revealed an ionic interaction between the SNRIs amino group and residue Asp98 (hSERT) or Asp75 (hNET). As illustrated in SI, Figure S5, the four studied SNRIs (desvenlafaxine, duloxetine, levomilnacipran, and venlafaxine) fitted into the S1 drug binding site surrounded by the regions of TM1, 3, 6, 8, and 10. Prior to docking, the validation of an appropriate docking protocol was required. Since desvenlafaxine and duloxetine had been cocrystallized together with LeuBAT (PDB code 4MM7 and 4MM6),[25] the cross-docking strategy was adopted herein to guarantee correct generation of a drug's initial pose by docking the cocrystallized desvenlafaxine into the structure of LeuBAT obtained with duloxetine bound (more details were provided in SI, Method S5), and the cocrystallized poses of desvenlafaxine and duloxetine were then superimposed to their corresponding cross-docking poses. Both poses were consistent with each other (SI, Figure S6), and RMSDs between the docked and cocrystallized poses of desvenlafaxine and duloxetine were 1.18 and 1.65 Å, respectively. Moreover, the docking conformations of the hSERT and hNET models in complex with desvenlafaxine and duloxetine were also aligned to the crystal structures 4MM7 and 4MM6 (SI, Figure S7). The aligned results showed that, except for the docking pose of desvenlafaxine in hNET (RMSD = 2.07 Å), the RMSDs of the other three poses were all below 2 Å. Therefore, the cross-docking results between 2MM7 and 4MM6 and the comparison of desvenlafaxine and duloxetine docking poses in hSERT and hNET with their cocrystallized pose in LeuBAT guaranteed the correct initial poses of the four studied SNRIs generated in this work.

Assessment of SNRIs Binding to hSERT and hNET. *MD Simulations.* Accuracy and reliability of SNRIs docking poses in S1 sites of hSERT and hNET were accessed by all atom explicit solvent MD simulation, and a total of 1.2 μs simulation trajectories was collected. Compared to initial conformation, RMSDs of protein backbone and ligand heavy atoms over the course of simulations were calculated and plotted in SI, Figure S8. As shown, all simulation complexes underwent relatively small conformation changes (RMSD < 3 Å). The small fluctuation of average RMSD of protein backbone atoms (2.09−2.83 Å, Table S1) indicated that each complex reached an equilibrium state. Moreover, the average RMSD of the binding site backbone atoms (1.07−1.48 Å, Table S1) and ligand heavy atoms (0.50−1.48 Å, Table S1) demonstrated that the predicted SNRIs poses were compatible with the S1 site of hSERT and hNET.

DOI: 10.1021/acschemneuro.7b00490
ACS Chem. Neurosci. 2018, 9, 1128−1140

Table 2. Calculated and Experimental Binding Energies of Four Studied SNRIs Binding to the Wild-type hSERT and hNET[a]

SNRIs	targets	K_i[b]	ΔG_{exp}[c]	$\Delta\Delta G_{exp}$[d]	ΔG_{calc}[e]	$\Delta\Delta G_{calc}$[d]
desvenlafaxine	hSERT	40.2[19]	−10.09	−2.44	−42.04 ± 0.12	−2.49
	hNET	558.4[19]	−8.53	−0.88	−42.02 ± 0.11	−2.47
duloxetine	hSERT	0.8[44]	−12.42	−4.77	−49.04 ± 0.12	−9.49
	hNET	7.5[44]	−11.09	−3.44	−47.61 ± 0.13	−8.06
levomilnacipran	hSERT	11.2[43]	−10.85	−3.20	−43.81 ± 0.11	−4.26
	hNET	92.2[43]	−9.60	−1.95	−41.38 ± 0.11	−1.83
venlafaxine	hSERT	82[44]	−9.68	−2.03	−41.96 ± 0.15	−2.41
	hNET	2480[44]	−7.65	0	−39.55 ± 0.11	0

[a]ΔG is in kcal/mol, and K_i value is in nM. [b]Experimental K_i value from reported work in refs 19, 43, and 44. [c]Estimated binding energy based on K_i values using $\Delta G_{exp} = RT \ln(K_i)$. [d]Binding energy difference was computed using $\Delta\Delta G = \Delta G - \Delta G_{venlafaxine}$. [e]Calculated binding energy in this work.

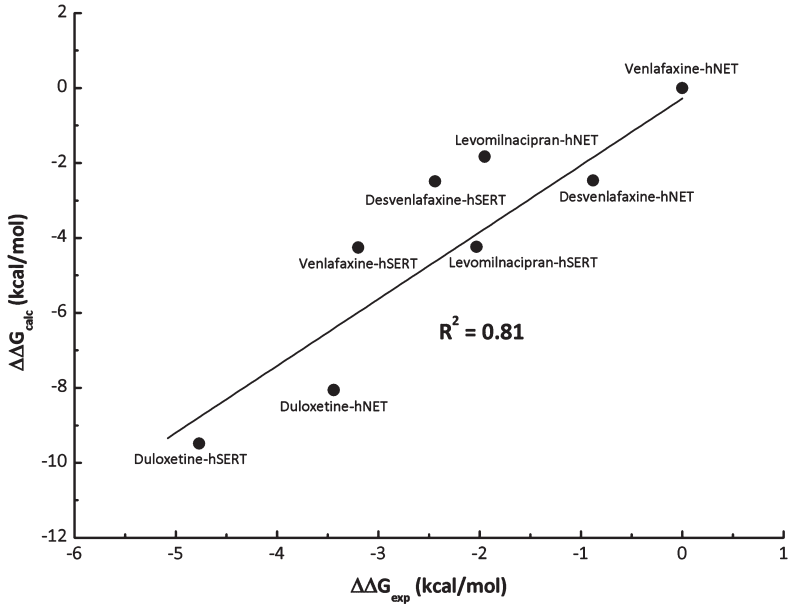

Figure 2. Correlation between the calculated binding energy differences ($\Delta\Delta G_{calc}$) and the experimental data ($\Delta\Delta G_{exp}$) estimated by K_i values for all studied complexes. The R^2 value equals 0.81.

Profiles of SNRIs Binding Free Energies in Complex with hSERT and hNET. To get the relative order of the binding free energy (ΔG_{calc}) of the studied SNRIs, the MM/GBSA method was used to calculate ΔG_{calc} of hSERT and hNET in complex with desvenlafaxine, duloxetine, venlafaxine, and levomilnacipran. Meanwhile, the experimental binding affinity (ΔG_{exp}) was calculated based on the reported K_i values[19,43,44] via $\Delta G_{exp} = RT \ln(K_i)$. The results of calculations are summarized in Table 2 (more details of each free energy term in SI, eq S1 are shown in SI, Table S2). As shown in Table 2, ΔG_{calc} values in this work were overestimated compared to those of experiment (ΔG_{exp}), and the main reason for this overestimation came from the exclusion of entropic contribution. Nevertheless, for ligands with similar structures and target binding modes, the entropy contribution could be omitted if one was only interested in the relative order of binding affinities.[45] Moreover, the feasibility of excluding entropic contribution from this study was validated by the similar binding mode of the studied SNRIs in both hSERT and hNET revealed by MD simulation. As a result, linear fit of relative binding free energies between $\Delta\Delta G_{calc}$ and $\Delta\Delta G_{exp}$ of four studied SNRIs gave a strong correlation (R^2 = 0.81, as illustrated in Figure 2), which indicated that the ascending trend of binding affinities from experiment was reproduced very well by ΔG_{calc} in this work.

Validation of the Simulation Models. Besides the good correlation between the results of simulation and experiment discovered in the previous section, three lines of evidence were collected to further validate the constructed simulation models.

Evidence 1: Sensitivity Profile Identified by in Silico Site-Directed Mutagenesis Analysis. The sensitivity profiles were expected to give great insight into the binding mechanism of SNRIs.[30] The sensitivity of certain residue to SNRIs binding could be estimated by difference in the calculated binding energy before and after *in silico* mutation. In this study, the sensitivity profiles of eight mutations (Y95A, I172M, F341Y, and S438T in hSERT; F72Y, V148I, F323Y, and S419T in hNET) for two SNRIs (duloxetine and venlafaxine) characterized by previous experiments[30] were selected, and their sensitivities were explored by *in silico* mutation and MD simulation on the resulting wild-type models (SI, Figure S10). The calculated binding free energies of those two SNRIs and the fold-changes in their binding affinities from Sorensen's experiments[30] induced by those aimed mutations are shown in Table 3, and information on each energy term is listed in SI, Table S3. As shown, sensitivity profiles of eight mutations reported in Sorensen's work[30] were successfully predicted by the calculated $\Delta\Delta G_{calc}$. Particularly, simulation revealed S438T in hSERT and F72Y, V148I, F323Y, and S419T in hNET as

DOI: 10.1021/acschemneuro.7b00490
ACS Chem. Neurosci. 2018, 9, 1128−1140

Table 3. Calculated and Experimental Changes in Binding Energies of 16 SNRIs Bonded hSERT and hNET Complexes[a] before and after Those Mutations in hSERT and hNET[30b]

SNRIs	targets	mutations	$\Delta\Delta G_{calc}$[c]	FC_{calc}[d]	FC_{exp}[e]	$\Delta\Delta G_{exp}$[f]
venlafaxine	hSERT	Y95A	2.08	33.42	73.89 (47.15−126.57)	2.55
		I172M	2.31	49.27	100.27 (59.27−181.03)	2.73
		F341Y	0.62	2.85	5.87 (3.62−10.31)	1.05
		S438T	−0.52	0.42	0.59 (0.35−1.08)	−0.31
	hNET	F72Y	−0.32	0.58	0.97 (0.86−1.08)	−0.02
		V148I	−1.03	0.18	0.05 (0.04−0.07)	−1.78
		F323Y	0.69	3.2	1.50 (1.24−1.79)	0.24
		S419T	0.49	2.29	2.59 (2.11−3.11)	0.56
duloxetine	hSERT	Y95A	1.59	14.62	24.00 (21.18−27.21)	1.88
		I172M	1.34	9.59	24.85 (21.00−29.24)	1.9
		F341Y	0.26	1.55	2.37 (1.91−2.89)	0.51
		S438T	−0.55	0.4	0.45 (0.35−0.57)	−0.47
	hNET	F72Y	0.02	1.03	1.23 (0.74−2.03)	0.12
		V148I	−0.81	0.25	0.19 (0.13−0.27)	−0.98
		F323Y	0.56	2.57	3.12 (1.92−5.06)	0.67
		S419T	−0.39	0.52	0.80 (0.58−1.16)	−0.13

[a]Two SNRIs against eight single-point mutations. [b]ΔG is in kcal/mol. See SI Table S3 for details of each energy term. [c]$\Delta\Delta G_{calc} = \Delta G_{mutation} - \Delta G_{wild\text{-}type}$. [d]Fold-changes of potency (FC_{calc}) were derived from $\Delta\Delta G_{calc}$ by the equation $\Delta\Delta G_{calc} = RT \ln(FC_{calc})$. [e]Fold-changes of potency (FC_{exp}) measured by K_i values ($FC_{exp} = K_i(mutation)/K_i(wild\text{-}type)$).[30] Numbers outside the parentheses indicate the fold-changes derived from the mean experimental values of both K_i(mutation) and K_i(wild-type). The first number in the parentheses indicates the minimum fold-change, while the second one indicates the maximum fold-change. [f]$\Delta\Delta G_{exp}$ were derived from the FC_{exp} from the equation $\Delta\Delta G_{exp} = RT \ln(FC_{exp})$.

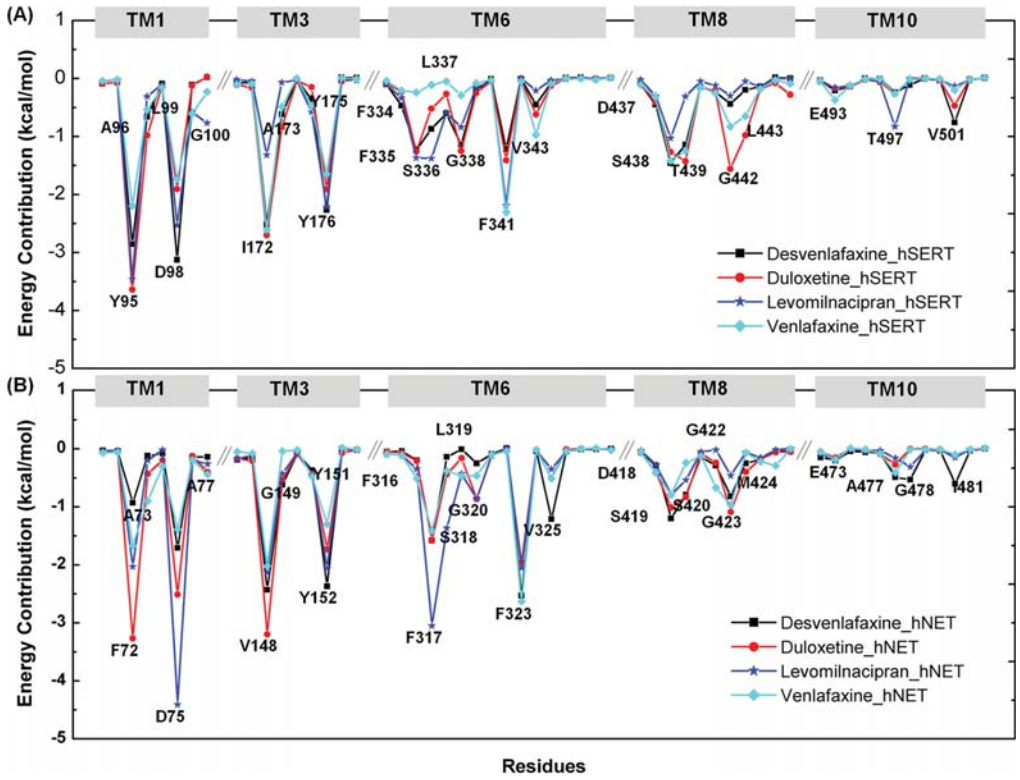

Figure 3. Per-residue contributions of binding energies of the eight studied complexes. To get a clear view, only residues in proximity of the drug binding sites (TM1, TM3, TM6, TM8, and TM10) are shown.

nonsensitive mutations (<5-fold change in binding affinity) to both studied SNRIs. In Table 3, the $\Delta\Delta G_{calc}$ values were between −1.03 and 0.56 kcal/mol. The corresponding range of fold-change in potency (FC_{calc}) could thus be estimated as 0.01 to 2.57 by $\Delta\Delta G_{cal} = RT \ln(FC_{calc})$, which were comparable to the experimentally estimated nonsensitive FC_{exp} (from 0.05 to 3.12).[30] Meanwhile, Y95A and I172M in hSERT were found to be sensitive (>5-fold change in binding affinity) to both SNRIs by this study, and their $\Delta\Delta G_{calc}$ values were between 1.34 and 2.08 kcal/mol. The corresponding range of FC_{calc} was estimated as from 9.59 to 33.42, which was also comparable to those experimentally estimated sensitive FC_{exp} (from 24.00 to

DOI: 10.1021/acschemneuro.7b00490
ACS Chem. Neurosci. 2018, 9, 1128−1140

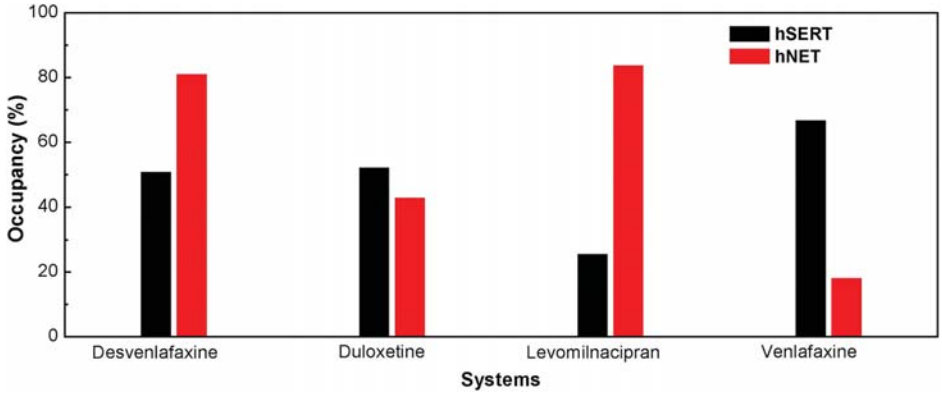

Figure 4. Analysis of hydrogen bonds between SNRIs and Asp98 (hSERT) or Asp75 (hNET). The hydrogen bonds are determined by the acceptor···donor atom distance of less than 3.5 Å and acceptor···H-donor angle of greater than 120°. Occupancy (%) represents the stability and strength of the hydrogen bonds.

100.27).[30] Finally, F341Y in hSERT was found to be sensitive to venlafaxine but nonsensitive to duloxetine, and the estimated FC_{calc} value was also comparable to the experimental result. Distinct difference in FC_{calc} between sensitive and nonsensitive mutations indicated that those constructed models were capable of distinguishing the sensitive mutations from the nonsensitive ones. As all *in silico* site-directed mutagenesis analyses were based on the models constructed in this work, their ability to identify the sensitivity profiles of hSERT and hNET residues could be considered as the first line of evidence for model validation. The conformational change in hSERT and hNET binding pocket as well as shift of two SNRIs accommodating into the pocket are shown in SI, Figure S10.

Evidence 2: hSERT's Crystal Structure Reproduced by MD Simulation. The recently determined X-ray structure of hSERT[35] could be used as a valuable reference for validating the simulation models in this work. As shown in Table 1 and SI, Figure S3A, hSERT's homology model generated in this study demonstrated substantial resemblance to the reported hSERT X-ray structure as indicated by a relatively low RMSD (2.45 Å). More importantly, the superimposition of the constructed hSERT model with the reported hSERT crystal structure showed significant structural similarity (RMSD = 0.80 Å) in the S1 binding site (SI, Figure S3B). These data demonstrated that the hSERT models generated on the basis of the dDAT crystal structure could serve as accurate platforms for exploring SNRIs binding at the hSERT binding site. To further support this conclusion, MD simulation and binding energy calculation of hSERT's cocrystallized structure in complex with a typical SSRI drug, escitalopram, were conducted,[36] and very consistent structure features (RMSDs of whole structure, S1 binding site, and ligand were 3.13, 1.01, and 1.23 Å, respectively) and a very similar value in binding free energy (RMSD was 0.20 kcal/mol) between the simulation and the X-ray structure[46] were observed. Taken together, the success in reproducing hSERT's crystal structure could be another line of evidence for model validation.

Evidence 3: Comparison of Results from Simulations with Experimental Structures of SNRIs in LeuBAT. The cocrystallized structures of LeuBAT (the engineered LeuT to harbor the human-like pharmacology) in complex with two approved SNRI drugs (desvenlafaxine and duloxetine) were determined by Wang et al.[25] Crystallographic analysis showed that these two chemically diverse inhibitors shared a remarkably similar binding mode. In particular, the amino groups of both desvenlafaxine and duloxetine interacted with Asp24 in LeuBAT (the corresponding residues Asp98 in hSERT and Asp75 in hNET).[25] Moreover, the cavity formed by Tyr21, Val104, Tyr108, and Phe259 (the corresponding residues Tyr95, Ile172, Tyr176, and Phe341 in hSERT; Phe72, Val148, Tyr151, and Phe317 in hNET) was occupied by duloxetine's naphthalene ring and desvenlafaxine's cyclohexanol ring.[25] Duloxetine's thiophene ring and desvenlafaxine's phenol ring were involved in the subsite comprised of Phe253, Asp404, and Thr408 (the corresponding residues Phe335, Glu493, and Thr497 in hSERT; Phe323, Asp473, and Ala477 in hNET), which probably showed a role in enhancing inhibitor affinity and specificity.[25] In this study, all those mentioned residues were identified as high contribution ones for the binding of the studied SNRIs (see Figure 3), which could be the third line of evidence validating the resulting simulation models.

Analyzing the Binding Mode of SNRIs in hSERT and hNET. *Conserved Salt Bridge and Hydrogen Bond Anchoring SNRIs at the S1 Sites of hSERT and hNET.* Representative snapshots of hSERT and hNET complex bound with SNRIs from equilibrated MD trajectories are shown in SI, Figure S11. As shown, the salt bridge and hydrogen bond between the side chain of Asp in hSERT and hNET and the amino group of SNRIs were crucial for ligand binding and conserved across all studied SNRIs. First, the distances between salt bridge forming atoms ($-N^{+}\cdots OD-$) for the binding of desvenlafaxine, duloxetine, levomilnacipran, and venlafaxine were relatively stable (SI, Figure S12). Second, hydrogen bonds between SNRIs and the carboxyl group of Asp in S1 sites of hSERT and hNET are illustrated in Figure 4, and the high percentage occupancy demonstrated a stable hydrogen bond along the simulation with interaction distance of 2.56−2.85 Å and bond angle ranging from 144.13° to 164.79°. These results suggested that salt bridges and hydrogen bonds were conserved and required for anchoring the studied SNRIs at the S1 sites of hSERT and hNET.

Per-Residue Binding Free Energy Contributing to SNRIs Binding. To understand the interaction between SNRIs and hSERT and hNET, per-residue decomposition analysis was conducted to obtain a quantitative picture of each amino acid's free energy contribution to SNRIs binding. Herein, a plot (Figure 3) showing binding free energy contributions of each amino acid was generated. To the best of our knowledge,

DOI: 10.1021/acschemneuro.7b00490
ACS Chem. Neurosci. 2018, 9, 1128−1140

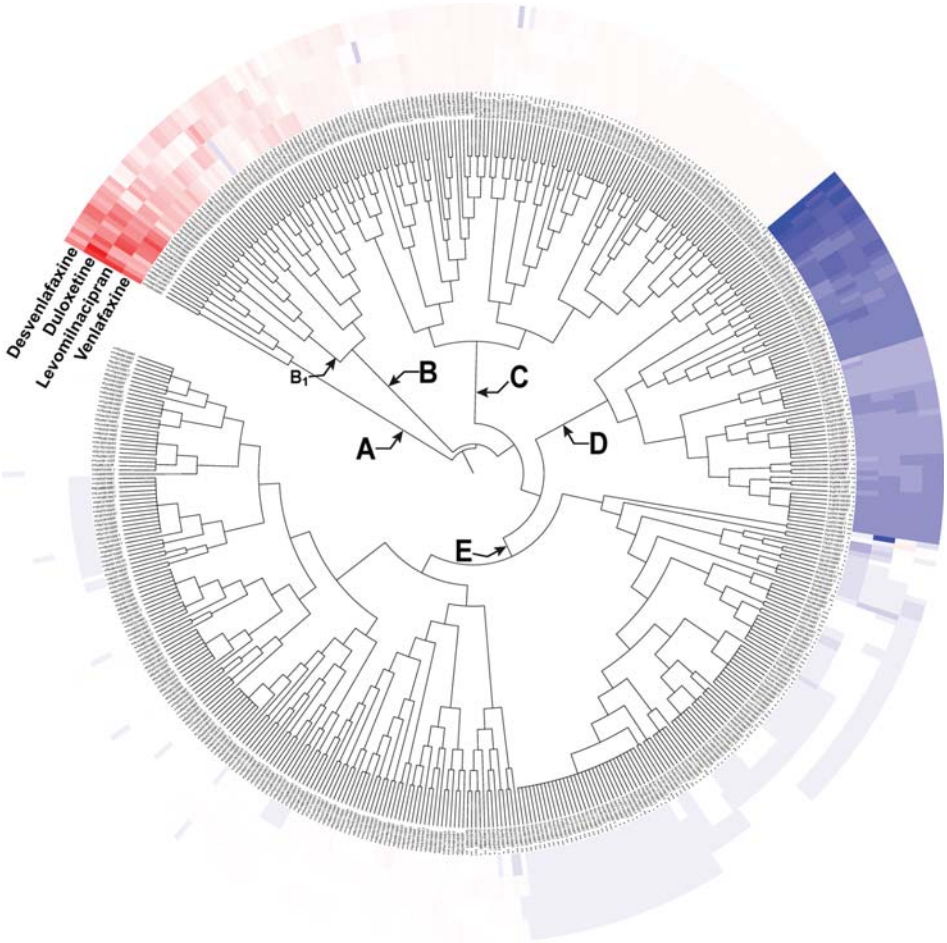

Figure 5. Clustering tree of 505 residues with contributions to at least one studied SNRI binding to hSERT and hNET. Residue binding energy contributions favoring SNRIs' binding are displayed in red, with the highest contribution set as exact red and the lower contributions gradually fading toward white color (no contribution). Residue energy contributions hampering SNRIs' binding are shown in blue, with the highest one set as exact blue and the lower ones gradually fading toward white color.

Figure 3 is the first report of SNRIs binding energy contribution on a per-residue basis. As shown, there were 14, 15, 14, and 12 residues in hSERT and 13, 12, 10, and 12 residues in hNET identified with high energy contribution (with the absolute energy contribution greater than or equal to 0.5 kcal/mol) for the binding of desvenlafaxine, duloxetine, levomilnacipran, and venlafaxine, respectively. On one hand, the energy contributions of hSERT and hNET residues to the same SNRI vary greatly (−0.57 kcal/mol for hNET Gly149 and −3.06 kcal/mol for hSERT Asp98 when binding desvenlafaxine), and energy contributions of the same residue to different SNRIs also differ significantly (the contributions of polar residue Asp98 in hSERT (Asp75 in hNET) were from −2.46 (−4.34) kcal/mol for levomilnacipran to −3.43 (−1.26) kcal/mol for venlafaxine). On the other hand, Figure 3 also infers a certain level of similarity among the four SNRIs, which inspired us to conduct a deeper exploration of the binding mode shared by all studied SNRIs approved by the U.S. FDA.

Binding Mode Shared by All Studied SNRIs Approved by FDA. The binding mode shared by approved SNRIs in hSERT and hNET provided a useful framework from which novel lead scaffolds could be assessed and discovered.[38,47] To identify the most favorable binding mode shared by all four approved SNRIs, hierarchical clustering with *ward algorithm*[48] was applied to identify key residues (hot spots) from those per-residue binding energies generated in the previous section. In particular, there were 1080 residues with energy contribution information for four studied SNRIs, 575 of which had no contribution (=0 kcal/mol) to the binding of any studied SNRI. Then, the energy contribution of the remaining 505 residues was used for clustering analysis. As shown by the hierarchical tree in Figure 5, five distinct residue groups (A, B, C, D, and E) were identified. Binding energy contributions favoring SNRIs binding are displayed in red, with the highest contribution (−4.34 kcal/mol) set as exact red and lower contributions gradually fading toward white (0 kcal/mol). Meanwhile, energy contributions hampering SNRIs binding are all colored in blue, with the highest one (0.17 kcal/mol) set as exact blue and lower ones gradually fading toward white. It is necessary to clarify that the absolute value of the highest contribution favoring SNRI binding (exact red) was 26 times stronger than that hampering the binding (exact blue).

The energy contribution of residues in group A (Tyr95, Asp98, Ile172, Tyr176, and Phe341 in hSERT; Phe72, Asp75, Val148, Tyr152, Phe317, and Phe323 in hNET) was consistently higher across all studied SNRIs and more favorable to binding than residues in other groups. For each SNRI, the sum of energy contributions of residues in group A constituted

DOI: 10.1021/acschemneuro.7b00490
ACS Chem. Neurosci. 2018, 9, 1128−1140

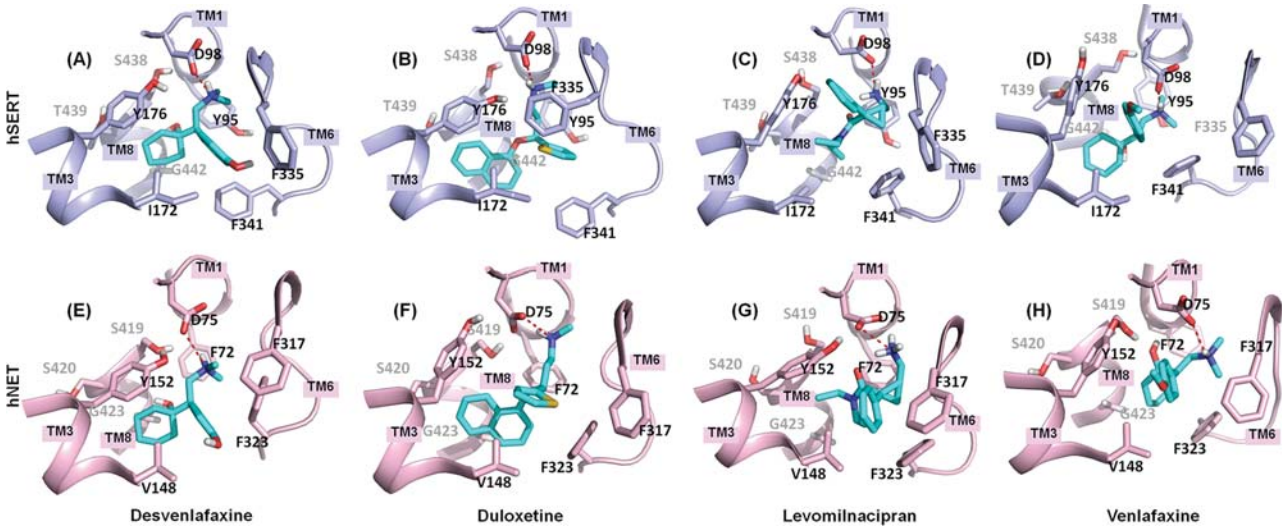

Figure 6. Binding modes of SNRIs in S1 binding site of hSERT and hNET that resulted from MD simulations. (A−D) 3D representation of binding interactions between SNRIs and hSERT. (E−F) 3D representation of binding interactions between SNRIs and hNET. Cartoon is used for the backbone atoms. Residues and ligands are shown in stick, and only polar hydrogen atoms are displayed for clarity. Salt bridges and hydrogen bonds are depicted as red dotted lines.

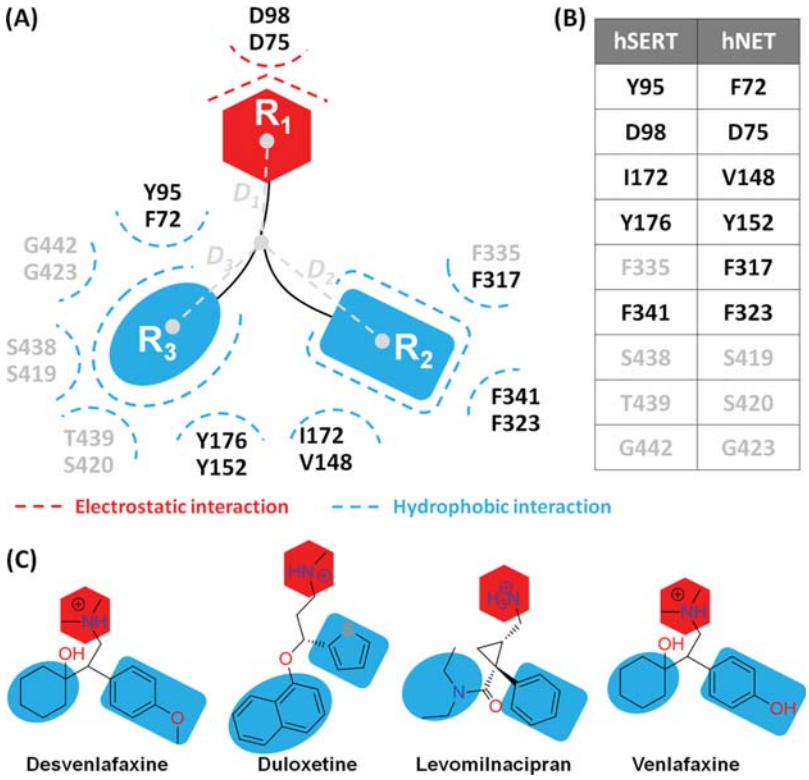

(B)

hSERT	hNET
Y95	F72
D98	D75
I172	V148
Y176	Y152
F335	F317
F341	F323
S438	S419
T439	S420
G442	G423

Figure 7. 2D schematic representation of the identified binding mode of four studied SNRIs in hSERT and hNET. The electrostatic and hydrophobic interactions are depicted in red and light blue dashed lines, respectively. The red color (R_1) indicates chemical group with electrostatic interaction to residues in the vicinity, while light blue (R_2) and (R_3) represents chemical groups with only hydrophobic interactions to their nearby residues. Each chemical group was generalized by superimposition of four SNRIs in the S1 pocket. The residues in dark text (Tyr95, Asp98, Ile172, Tyr176, and Phe341 in hSERT; Phe72, Asp75, Val148, Tyr152, Phe317, and Phe323 in hNET) belong to subgroup A (Figure 5), and the residues in gray (Phe335, Ser438, Thr439, and Gly442 in hSERT; Ser419, Ser420, and Gly423 in hNET) aare clustered into subgroup B_1 (Figure 5).

the primary portion of total energy (hSERT, 47.14% for desvenlafaxine, 40.36% for duloxetine, 48.48% for levomilnacipran, and 48.47% for venlafaxine; hNET, 49.53% for desvenlafaxine, 53.93% for duloxetine, 59.31% for levomilnacipran, and 48.90% for venlafaxine). In the meantime, the sum of energy contributions of residues in subgroup B_1 (Ala96, Ala173, Phe335, Ser336, Glu338, Ser438, Thr439, and Gly442 in hSERT; Ala145, Val325, Ser419, Ser420, and Gly423 in hNET)

DOI: 10.1021/acschemneuro.7b00490
ACS Chem. Neurosci. 2018, 9, 1128−1140

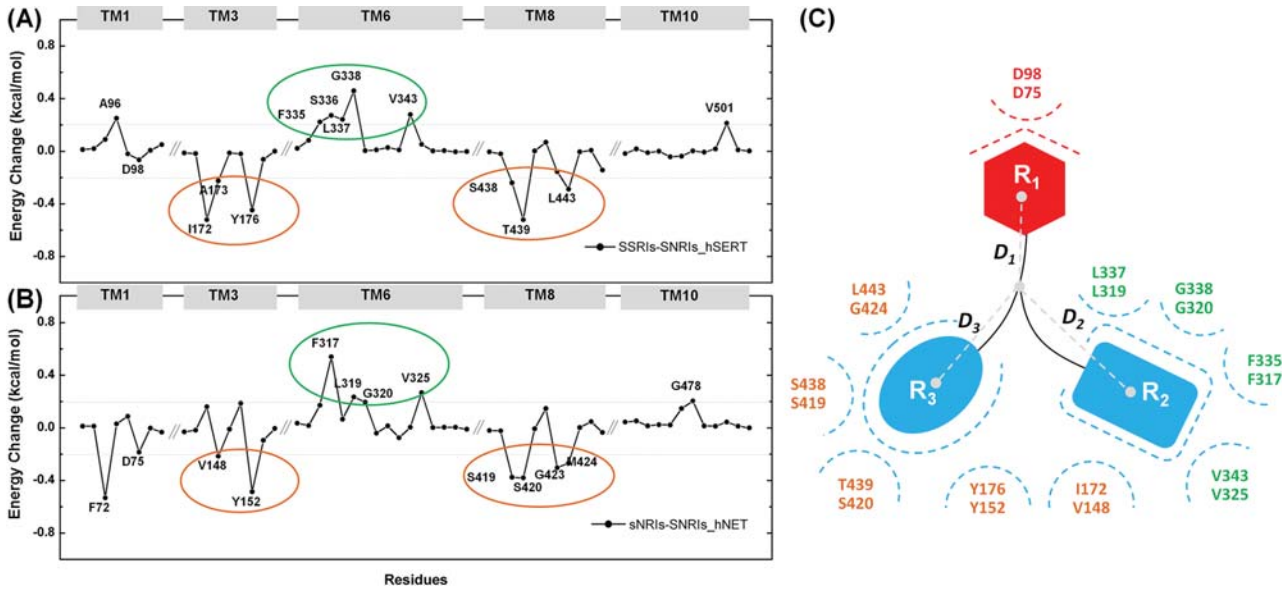

Figure 8. Changes of the mean energy contribution of residues (A) between SSRIs and SNRIs in hSERT and (B) between sNRIs and SNRIs in hNET. Only residues in the proximity of the drugs' S1 binding sites (TM1, TM3, TM6, TM8, and TM10) are shown. (C) Residues in the TM3 and TM8 regions contributed more energy to the binding of SSRIs and sNRIs than that of SNRIs (labeled in orange), and residues in the TM6 region contributed more energy to the binding of SNRIs than that of SSRIs and sNRIs (labeled in green) and were mapped to the shared binding mode identified for all approved SNRIs.

offered 27.96%, 31.49%, 22.97%, and 27.71% of total free energies for the binding of desvenlafaxine, duloxetine, levomilnacipran, and venlafaxine in hSERT and 20.68%, 15.97%, 11.06%, and 13.61% of the total energy for binding desvenlafaxine, duloxetine, levomilnacipran, and venlafaxine with hNET, respectively. In this study, residues in subgroups A and B_1 were identified as the hot spots with "strong" and "relatively strong" contributions. Taken together, 13 hot spots in hSERT and 11 hot spots in hNET revealed a similar pattern shared by those studied SNRIs in spite of their distinct structures. Moreover, among those residues, 9 residues (Tyr95, Asp98, Ile172, Tyr176, Phe335, Phe341, Ser438, Thr439, and Gly442 in hSERT; Phe72, Asp75, Val148, Tyr152, Phe317, Phe323, Ser419, Ser420, and Gly423 in hNET) were hot spots shared by the studied SNRIs binding to both hSERT and hNET.

The conformational features of how SNRIs were accommodated into 9 hot spot residues are shown in Figure 6. A pocket was defined by hot spots with a slight conformational shift, and all SNRIs fitted the pocket with a similar orientation. Thus, the binding mode of SNRIs−hSERT and −hNET recognition is generalized and schematically represented in Figure 7. As shown, the shared binding mode was defined by collective electrostatic and hydrophobic interactions between three chemical groups (R_1, R_2 and R_3) and 9 hot spots (Tyr95, Asp98, Ile172, Tyr176, Phe335, Phe341, Ser438, Thr439, and Gly442 in hSERT; Phe72, Asp75, Val148, Tyr152, Phe317, Phe323, Ser419, Ser420, and Gly423 in hNET). In Figure 6 and Figure 7, hot spots with strong and relatively strong contributions are shown in black and gray color, respectively. The chemical groups in Figure 7 are highlighted in red and light blue. R_1 formed electrostatic interactions with Asp98 (hSERT) and Asp75 (hNET), R_2 offered hydrophobic interactions with Tyr95, Ile172, Tyr176, Ser438, Thr439, and Gly442 (hSERT) and Phe72, Val148, Tyr152, Ser419, Ser420, and Gly423 (hNET), while R_3 contacted Ile172, Tyr176, Phe335, and Phe341 (hSERT) and Val148, Tyr152, Phe317, and Phe323 (hNET).

Identifying the Key Properties Discriminating SNRIs from SSRIs and sNRIs. *Per-Residue Energies Differentially Contributing to the Binding of SNRIs, SSRIs, and sNRIs.* Homology model of hSERT and hNET showed similar molecular architecture (Figure 1B). Their amino acid sequence shared an overall identity of 54% (Figure S1) and an S1 binding site identity of 62% (SI, Figure S13). The identification of the key properties determining drug selectivity in target binding was critical for the development of antidepressants with improved efficacy.[49−53] Although crystallography,[25,54] mutagenesis[29,30] studies, and molecular modeling[32,33,55,56] on antidepressants were extensively explored, the key properties determining drug selectivity remained elusive. To discover key physicochemical properties of SNRIs underlying their dual-targeting mechanism, the per-residue energies contributing to SNRIs binding were calculated and compared with those of SSRIs and sNRIs reported in previous studies.[33,46] In particular, the changes of per-residue energy between SSRIs and SNRIs binding to hSERT are plotted in Figure 8A, and the changes of per-residue energy between sNRIs and SNRIs binding to hNET are depicted in Figure 8B. Moreover, a schematic representation of key residues differentially contributing to the binding of SNRIs and SSRIs/sNRIs is provided in Figure 8C. As shown, the increased energy contribution of the residues in the TM6 region (Phe335, Leu337, Gly338, and Val343 in hSERT and Phe317, Leu319, Gly320, and Val325 in hNET) is required for the SNRIs dual-targeting mechanism (Figure 8A,B) by interacting with the R_2 group of SNRIs (Figure 8C). In contrast, residues in the TM3 and TM8 regions (Ile172, Tyr176, Ser438, Thr439, and Leu443 in hSERT and Val148, Tyr152, Ser419, Ser420, and Met424 in hNET) offered more to SSRIs and sNRIs binding (Figure 8A,B) and mainly located around the R_3 group of both SSRIs and sNRIs (Figure 8C). Among those residues, except for Ser438 (hSERT) and Ser149

DOI: 10.1021/acschemneuro.7b00490
ACS Chem. Neurosci. 2018, 9, 1128−1140

(hNET), several nonconserved ones (Ile172, Thr439, and Leu443 in hSERT and Val148, Ser420, and Met424 in hNET) have been reported as molecular determinants controlling antidepressant binding selectivity and further validated by the site-mutagenesis studies.[54,55] Meanwhile, simulation revealed that Asp98 in hSERT (Asp75 in hNET) was essential for the recognition of SSRIs, sNRIs, and SNRIs in hSERT and hNET.[25] As shown, no obvious change in energy contribution of Asp98 in hSERT (Asp75 in hNET) for the binding of SSRIs,[46] sNRIs,[46] and SNRIs was observed (Figure 8). Therefore, these interactions should be preserved in the binding of antidepressants as a prerequisite.

Identifying the Key Moiety of SNRIs Determining Their Dual-Targeting Mechanism. Based on simulation results, the binding mode of approved SSRIs,[46] sNRIs,[33] and SNRIs in hSERT and hNET was defined by the collective electrostatic and hydrophobic interactions between 3 chemical groups (R_1, R_2, and R_3) and the corresponding residues in the S1 binding site (Figure 7). As reported, the moieties should be the determinants of the SNRIs mode of action,[49] but it is unclear how a specific moiety contributes to the SNRIs dual-targeting mechanism. Herein, the distances between drug centroid and the centroids of the 3 drug moieties (R_1, R_2, and R_3) were measured and summarized based on the 3D conformation of approved SNRIs, SSRIs, and sNRIs in the S1 binding pocket (Table 3 and SI, Table S5). As demonstrated in Figure 7 and Table 4, D_1, D_2, and D_3 indicated the mean distances between drug centroid and the centroids of drug moiety R_1, R_2, and R_3, respectively. As shown, D_2 of SNRIs (3.18 Å) was longer than that of SSRIs (3.11 Å) and sNRIs (3.01 Å), while D_3 of SNRIs (2.93 Å) was much shorter than that of SSRIs (3.70 Å) and sNRIs (3.31 Å). Meanwhile, Figure 7 showed that R_2 mainly interacted with residues located in TM6 of the protein and R_3 mainly contacted residues located in TM3 and TM8. Based on these results, it was reasonable to speculate that the distances between SNRIs centroid and centroids of their aromatic rings (R_2 and R_3), which reflected the depth of aromatic rings stretching into the hydrophobic pocket, were closely related to the SNRIs dual-targeting mechanism.

Table 4. Mean Distances between the Centroid of All Approved SNRIs, SSRIs and sNRIs and the Centroids of their R_1, R_2, and R_3 Groups as Described in Figure 7

distance (Å)	SNRIs	SSRIs[a]	sNRIs[a]
D_1	3.51	3.69	4.09
D_2	3.18	3.11	3.01
D_3	2.93	3.70	3.31

[a]The data was obtained from our previous studies.[33,46]

CONCLUSIONS

This study aimed at revealing the SNRIs dual-targeting mechanism by comparing their binding mode in hSERT and hNET with those of SSRIs and sNRIs. By adopting an integrated computational method, the binding mode shared by 4 FDA approved SNRIs in their corresponding targets was discovered, and several key residues were identified as different in their per-residue energy contributions to the binding of the SNRIs, SSRIs, and sNRIs. Based on these analyses, the distances between SNRIs centroids and the centroids of their aromatic rings (R_2 and R_3) were discovered and speculated as closely related to the SNRIs dual-targeting mechanism. Such findings provide a blueprint for assessing and discovering novel, safer, and more effective dual-targeting scaffolds for not only MDD but also other psychiatric disorders.

MATERIALS AND METHODS

System Setup. *Homology modeling of hSERT and hNET.* The sequences of hSERT, hNET and dDAT were first aligned using *ClustalW2*.[57] Then, using the X-ray crystal structure of dDAT (PDB code 4M48,[25] from Glu26 to Asp599) as template, the homology models of hSERT and hNET were constructed by the automated mode *SWISS-MODEL*.[58] The *PROCHECK*[59] was applied to evaluate the stereo chemical quality of the constructed hSERT and hNET models. Finally, two functional Na^+ in 4M48 were manually fitted into their corresponding binding sites in hSERT and hNET using the structure superimposition module of the *PyMOL* program.[60]

Docking SNRIs into hSERT and hNET. To get drug binding complexes, four FDA approved SNRIs (desvenlafaxine, duloxetine, levomilnacipran, venlafaxine) were docked into the modeled hSERT and hNET proteins using *Glide*.[61] First, Structures of 4 SNRIs were preprocessed by the *LigPrep*[62] using OPLS-2005 force field.[63] The ionized state was assigned by *Epik*[64] at a pH value of 7.0 ± 2.0. Then, hSERT and hNET homology models were prepared by adding hydrogen atoms, assigning partial charges and protonation states, and minimizing the structure using Protein Preparation Wizard module in *Maestro*.[65] Third, the docking grid boxes were defined by the residues (Tyr95, Asp98, Ile172, Asn177, Phe341 and Ser438 of hSERT and Phe72, Asp75, Val48, Gly149, Phe323 and Ser419 of hNET) identified as determinants for SNRIs binding[30] (more details were provided in SI, Method S1). Finally, the prepared SNRIs were docked into the defined binding pockets in both hSERT and hNET and the docking poses oriented in similar way as SSRIs/SNRIs cocrystallized with LeuBAT[25] were selected for MD simulation and thermodynamic analysis, and formed ionic interaction between amino group and Asp98 (hSERT) or Asp75 (hNET). Similar protocol was adopted in previously studies.[33,46]

Constructing the protein−ligand/membrane-water complex. The initial conformations of eight complexes obtained by docking were preoriented in *OPM*[66] with respect to the Membrane Normal which is defined by the *Z*-axis. Then the drug-target structures were further embedded into an explicit POPC lipid bilayer by Membrane Builder in *CHARMM-GUI*.[67] The TIP3P water[68] of 20 Å thickness was placed above and below the constructed bilayer. Environmental salt concentration was kept at 0.15 M by adding Na^+ and Cl^-. The overall system contained a total of ∼96,000 atoms per one periodic cell, and the box size was set as 83 Å × 83 Å × 127 Å.

MD Simulation and Thermodynamic Analysis. Starting from initial conformation of each complex produced by docking, MD simulation was performed to improve the fit of drugs into targets' binding pocket.[69] Simulations were conducted by GPU-accelerated PMEMD integrated in *AMBER14* package.[70] For each MD simulation, a sophisticated protocol including the minimization, heating and equilibration was employed (more details were provided in SI, Method S2). Then, 150 ns production NPT MD simulation was conducted with periodic boundary conditions at 310 K and 1Bar. The direct space interaction was calculated by considering long-range electrostatic interactions (cutoff = 10 Å) using the particle-mesh Ewald (PME) method.[71] All bonds involving hydrogen atoms were constrained by SHAKE algorithm[72] allowing an integration time step of 2 fs.

Based on the last 50 ns equilibrated production simulations, the binding free energies (ΔG_{calc}) of SNRIs to their targets (hSERT and hNET) were calculated by MM/GBSA method[68] (more details were provided in SI, Method S3). Comparing with absolute binding free energies with alchemical method,[73] endpoint calculation was more computationally effective to reproduce the relative order of ligands binding to one protein family.[74−79] To quantitatively evaluate the contribution of each residue to SNRIs' binding, the total binding energy was decomposed on a per-residue basis (more details were provided in SI, Method S4).

DOI: 10.1021/acschemneuro.7b00490
ACS Chem. Neurosci. 2018, 9, 1128−1140

Hierarchical Clustering Analysis. The hierarchical clustering tree of 505 residues with contributions to at least one studied SNRI binding on hSERT and hNET was generated based on per-residue energy contribution vectors using *R* statistical analysis software[80] with the similarity levels among vectors measured by the *Manhattan* distance:

$$\text{Distance(a,b)} = \sum_i |a_i - b_i| \quad (1)$$

where i denotes each dimension of per-residue energies a and b. Cluster algorithm used here is the Ward's minimum variance method,[48] which is designed to minimize the total within-cluster variance. The Ward's minimum variance module in the *R* package[80] was used, and the hierarchical tree graph was generated using the online tree generator iTOL.[81]

■ ASSOCIATED CONTENT

Supporting Information

The Supporting Information is available free of charge on the ACS Publications website at DOI: 10.1021/acschemneuro.7b00490.

Descriptions of methods used in this study; average RMSD value of the MD simulation; comparison of calculated and experimental binding energies of drug; energy terms calculated in mutation analysis; hydrogen bond analysis; distances between the centroids of drug and its R_1, R_2 and R_3 groups; sequence alignment of hSERT, hNET, and dDAT; Ramachandran plots of homology models; comparison of homology models constructed based on different templates; docking/cross-docking poses of studied drugs; RMSD of the MD simulation; conformation comparison of the mutation analysis; representative snapshot of drug−target interaction; distance of the salt bridge interaction; sequence alignment of the S1 binding site between hSERT and hNET (PDF)

■ AUTHOR INFORMATION

Corresponding Author

*Mailing address: Innovative Drug Research and Bioinformatics Group, College of Pharmaceutical Sciences, Zhejiang University, Hangzhou 310058, China. E-mail: zhufeng.ns@gmail.com, zhufeng@zju.edu.cn. Phone: +86-(0)571-8820-8444.

ORCID

Weiwei Xue: 0000-0002-3285-0574

Xiaojun Yao: 0000-0002-8974-0173

Feng Zhu: 0000-0001-8069-0053

Author Contributions

W.X., F.Y., P.W., G.Z., and F.Z. performed the research. W.X., Y.C., X.Y., and F.Z. analyzed data. F.Z. and W.X. designed the research and wrote the manuscript. All authors reviewed the manuscript.

Funding

Supported by Precision Medicine Project of the National Key Research and Development Plan of China (2016YFC0902200), National Natural Science Foundation of China (21505009), Innovation Project on Industrial Generic Key Technologies of Chongqing (cstc2015zdcy-ztzx120003), and Fundamental Research Funds for Central Universities (10611CDJXZ238826, CDJZR14468801, CDJKXB14011).

Notes

The authors declare no competing financial interest.

■ ABBREVIATIONS

dDAT, *Drosophila melanogaster* dopamine transporter; hNET, human norepinephrine transporter; hSERT, human serotonin transporter; MD, molecular dynamics; MDD, Major Depressive Disorder; MM/GBSA, Molecular Mechanics Generalized Born Surface Area; sNRIs, selective norepinephrine reuptake inhibitors; SNRIs, serotonin−norepinephrine reuptake inhibitors; SSRIs, selective serotonin reuptake inhibitors

■ REFERENCES

(1) Global Burden of Disease Study Collaborators (2015) Global, regional, and national incidence, prevalence, and years lived with disability for 301 acute and chronic diseases and injuries in 188 countries, 1990−2013: a systematic analysis for the Global Burden of Disease Study 2013. *Lancet 386*, 743−800.

(2) Chen, Y. Z., Zhu, F., Han, L. Y., Chen, X., Lin, H. H., Ong, S., Xie, B., and Zhang, H. L. (2008) Homology-free prediction of functional class of proteins and peptides by support vector machines. *Curr. Protein Pept. Sci. 9*, 70−95.

(3) Ramaker, M. J., and Dulawa, S. C. (2017) Identifying fast-onset antidepressants using rodent models. *Mol. Psychiatry 22*, 656−665.

(4) Zhu, F., Han, L., Zheng, C., Xie, B., Tammi, M. T., Yang, S., Wei, Y., and Chen, Y. (2009) What are next generation innovative therapeutic targets? Clues from genetic, structural, physicochemical, and systems profiles of successful targets. *J. Pharmacol. Exp. Ther. 330*, 304−315.

(5) Cai, X., Kallarackal, A. J., Kvarta, M. D., Goluskin, S., Gaylor, K., Bailey, A. M., Lee, H. K., Huganir, R. L., and Thompson, S. M. (2013) Local potentiation of excitatory synapses by serotonin and its alteration in rodent models of depression. *Nat. Neurosci. 16*, 464−472.

(6) Kristensen, A. S., Andersen, J., Jorgensen, T. N., Sorensen, L., Eriksen, J., Loland, C. J., Stromgaard, K., and Gether, U. (2011) SLC6 neurotransmitter transporters: structure, function, and regulation. *Pharmacol. Rev. 63*, 585−640.

(7) Yang, H., Qin, C., Li, Y. H., Tao, L., Zhou, J., Yu, C. Y., Xu, F., Chen, Z., Zhu, F., and Chen, Y. Z. (2016) Therapeutic target database update 2016: enriched resource for bench to clinical drug target and targeted pathway information. *Nucleic Acids Res. 44*, D1069−1074.

(8) Zhu, F., Zheng, C. J., Han, L. Y., Xie, B., Jia, J., Liu, X., Tammi, M. T., Yang, S. Y., Wei, Y. Q., and Chen, Y. Z. (2008) Trends in the exploration of anticancer targets and strategies in enhancing the efficacy of drug targeting. *Curr. Mol. Pharmacol. 1*, 213−232.

(9) Zhu, F., Shi, Z., Qin, C., Tao, L., Liu, X., Xu, F., Zhang, L., Song, Y., Liu, X., Zhang, J., Han, B., Zhang, P., and Chen, Y. (2012) Therapeutic target database update 2012: a resource for facilitating target-oriented drug discovery. *Nucleic Acids Res. 40*, D1128−1136.

(10) Li, Y. H., Yu, C. Y., Li, X. X., Zhang, P., Tang, J., Yang, Q., Fu, T., Zhang, X., Cui, X., Tu, G., Zhang, Y., Li, S., Yang, F., Sun, Q., Qin, C., Zeng, X., Chen, Z., Chen, Y. Z., and Zhu, F. (2018) Therapeutic target database update 2018: enriched resource for facilitating bench-to-clinic research of targeted therapeutics. *Nucleic Acids Res. 46*, D1121.

(11) Caron, M. G., and Gether, U. (2016) Structural biology: Antidepressants at work. *Nature 532*, 320−321.

(12) Zhu, F., Qin, C., Tao, L., Liu, X., Shi, Z., Ma, X., Jia, J., Tan, Y., Cui, C., Lin, J., Tan, C., Jiang, Y., and Chen, Y. (2011) Clustered patterns of species origins of nature-derived drugs and clues for future bioprospecting. *Proc. Natl. Acad. Sci. U. S. A. 108*, 12943−12948.

(13) Artigas, F. (2013) Future directions for serotonin and antidepressants. *ACS Chem. Neurosci. 4*, 5−8.

(14) Zhu, F., Ma, X. H., Qin, C., Tao, L., Liu, X., Shi, Z., Zhang, C. L., Tan, C. Y., Chen, Y. Z., and Jiang, Y. Y. (2012) Drug discovery prospect from untapped species: indications from approved natural product drugs. *PLoS One 7*, e39782.

(15) Stahl, S. M., Grady, M. M., Moret, C., and Briley, M. (2005) SNRIs: their pharmacology, clinical efficacy, and tolerability in comparison with other classes of antidepressants. *CNS Spectr. 10*, 732−747.

(16) Dreyfus, N., Myers, J. K., Badescu, V. O., de Frutos, O., de la Puente, M. L., Ding, C., Filla, S. A., Fynboe, K., Gernert, D. L., Heinz, B. A., Hemrick-Luecke, S. K., Johnson, K. W., Johnson, M. P., Lopez, P., Love, P. L., Martin, L. J., Masquelin, T., McCoy, M. J., Mendiola, J., Morrow, D., Muhlhauser, M., Pascual, G., Perun, T. J., Pfeifer, L. A., Phebus, L. A., Richards, S. J., Rincon, J. A., Seest, E. P., Shah, J., Shaojuan, J., Simmons, R. M., Stephenson, G. A., Tromiczak, E. G., Thompson, L. K., Walter, M. W., Weber, W. W., Zarrinmayeh, H., Thomas, C. E., Joshi, E., Iyengar, S., and Johansson, A. M. (2013) Discovery of a potent, dual serotonin and norepinephrine reuptake inhibitor. *ACS Med. Chem. Lett. 4*, 560−564.

(17) Xu, J., Wang, P., Yang, H., Zhou, J., Li, Y., Li, X., Xue, W., Yu, C., Tian, Y., and Zhu, F. (2016) Comparison of FDA Approved Kinase Targets to Clinical Trial Ones: Insights from Their System Profiles and Drug-Target Interaction Networks. *BioMed Res. Int. 2016*, 2509385.

(18) Tao, L., Zhu, F., Qin, C., Zhang, C., Xu, F., Tan, C. Y., Jiang, Y. Y., and Chen, Y. Z. (2014) Nature's contribution to today's pharmacopeia. *Nat. Biotechnol. 32*, 979−980.

(19) Deecher, D. C., Beyer, C. E., Johnston, G., Bray, J., Shah, S., Abou-Gharbia, M., and Andree, T. H. (2006) Desvenlafaxine succinate: A new serotonin and norepinephrine reuptake inhibitor. *J. Pharmacol. Exp. Ther. 318*, 657−665.

(20) Zhu, F., Han, B., Kumar, P., Liu, X., Ma, X., Wei, X., Huang, L., Guo, Y., Han, L., Zheng, C., and Chen, Y. (2010) Update of TTD: Therapeutic Target Database. *Nucleic Acids Res. 38*, D787−791.

(21) Tao, L., Zhu, F., Xu, F., Chen, Z., Jiang, Y. Y., and Chen, Y. Z. (2015) Co-targeting cancer drug escape pathways confers clinical advantage for multi-target anticancer drugs. *Pharmacol. Res. 102*, 123−131.

(22) Cuboni, S., and Hausch, F. (2014) Snapshot of antidepressants at work: the structure of neurotransmitter transporter proteins. *Angew. Chem., Int. Ed. 53*, 5008−5009.

(23) Rudnick, G. (2007) What is an antidepressant binding site doing in a bacterial transporter? *ACS Chem. Biol. 2*, 606−609.

(24) Yamashita, A., Singh, S. K., Kawate, T., Jin, Y., and Gouaux, E. (2005) Crystal structure of a bacterial homologue of Na+/Cl−dependent neurotransmitter transporters. *Nature 437*, 215−223.

(25) Penmatsa, A., Wang, K. H., and Gouaux, E. (2013) X-ray structure of dopamine transporter elucidates antidepressant mechanism. *Nature 503*, 85−90.

(26) Nolan, T. L., Geffert, L. M., Kolber, B. J., Madura, J. D., and Surratt, C. K. (2014) Discovery of novel-scaffold monoamine transporter ligands via in silico screening with the S1 pocket of the serotonin transporter. *ACS Chem. Neurosci. 5*, 784−792.

(27) Wang, P., Yang, F., Yang, H., Xu, X., Liu, D., Xue, W., and Zhu, F. (2015) Identification of dual active agents targeting 5-HT1A and SERT by combinatorial virtual screening methods. *Bio-Med. Mater. Eng. 1*, S2233−2239.

(28) Manepalli, S., Geffert, L. M., Surratt, C. K., and Madura, J. D. (2011) Discovery of novel selective serotonin reuptake inhibitors through development of a protein-based pharmacophore. *J. Chem. Inf. Model. 51*, 2417−2426.

(29) Andersen, J., Stuhr-Hansen, N., Zachariassen, L., Toubro, S., Hansen, S. M., Eildal, J. N., Bond, A. D., Bogeso, K. P., Bang-Andersen, B., Kristensen, A. S., and Stromgaard, K. (2011) Molecular determinants for selective recognition of antidepressants in the human serotonin and norepinephrine transporters. *Proc. Natl. Acad. Sci. U. S. A. 108*, 12137−12142.

(30) Sorensen, L., Andersen, J., Thomsen, M., Hansen, S. M., Zhao, X., Sandelin, A., Stromgaard, K., and Kristensen, A. S. (2012) Interaction of antidepressants with the serotonin and norepinephrine transporters: mutational studies of the S1 substrate binding pocket. *J. Biol. Chem. 287*, 43694−43707.

(31) Li, Y. H., Wang, P. P., Li, X. X., Yu, C. Y., Yang, H., Zhou, J., Xue, W. W., Tan, J., and Zhu, F. (2016) The Human Kinome Targeted by FDA Approved Multi-Target Drugs and Combination Products: A Comparative Study from the Drug-Target Interaction Network Perspective. *PLoS One 11*, e0165737.

(32) Koldso, H., Severinsen, K., Tran, T. T., Celik, L., Jensen, H. H., Wiborg, O., Schiott, B., and Sinning, S. (2010) The two enantiomers of citalopram bind to the human serotonin transporter in reversed orientations. *J. Am. Chem. Soc. 132*, 1311−1322.

(33) Zheng, G., Xue, W., Wang, P., Yang, F., Li, B., Li, X., Li, Y., Yao, X., and Zhu, F. (2016) Exploring the Inhibitory Mechanism of Approved Selective Norepinephrine Reuptake Inhibitors and Reboxetine Enantiomers by Molecular Dynamics Study. *Sci. Rep. 6*, 26883.

(34) Zhu, F., Li, X., Yang, S., and Chen, Y. (2018) Clinical success of drug targets prospectively predicted by in-silico study. *Trends Pharmacol. Sci.*, DOI: 10.1016/j.tips.2017.12.002.

(35) Coleman, J. A., Green, E. M., and Gouaux, E. (2016) X-ray structures and mechanism of the human serotonin transporter. *Nature 532*, 334−339.

(36) Nolan, T. L., Lapinsky, D. J., Talbot, J. N., Indarte, M., Liu, Y., Manepalli, S., Geffert, L. M., Amos, M. E., Taylor, P. N., Madura, J. D., and Surratt, C. K. (2011) Identification of a novel selective serotonin reuptake inhibitor by coupling monoamine transporter-based virtual screening and rational molecular hybridization. *ACS Chem. Neurosci. 2*, 544−552.

(37) Li, Y. H., Xu, J. Y., Tao, L., Li, X. F., Li, S., Zeng, X., Chen, S. Y., Zhang, P., Qin, C., Zhang, C., Chen, Z., Zhu, F., and Chen, Y. Z. (2016) SVM-Prot 2016: A Web-Server for Machine Learning Prediction of Protein Functional Families from Sequence Irrespective of Similarity. *PLoS One 11*, e0155290.

(38) Yan, A., Wang, L., Xu, S., and Xu, J. (2011) Aurora-A kinase inhibitor scaffolds and binding modes. *Drug Discovery Today 16*, 260−269.

(39) Monteggia, L. M., Malenka, R. C., and Deisseroth, K. (2014) Depression: the best way forward. *Nature 515*, 200−201.

(40) Lavecchia, A., and Cerchia, C. (2016) In silico methods to address polypharmacology: current status, applications and future perspectives. *Drug Discovery Today 21*, 288−298.

(41) Zhang, W., Pei, J., and Lai, L. (2017) Computational Multitarget Drug Design. *J. Chem. Inf. Model. 57*, 403−412.

(42) Faria, T. C., Cavalheiro, S., Hisaba, W. J., Moron, A. F., Torloni, M. R., Oliveira, A. L., and Borges, C. P. (2013) Improvement of motor function and decreased need for postnatal shunting in children who had undergone intrauterine myelomeningocele repair. *Arq. Neuro-Psiquiatr. 71*, 604−608.

(43) Auclair, A. L., Martel, J. C., Assie, M. B., Bardin, L., Heusler, P., Cussac, D., Marien, M., Newman-Tancredi, A., O'Connor, J. A., and Depoortere, R. (2013) Levomilnacipran (F2695), a norepinephrine-preferring SNRI: profile in vitro and in models of depression and anxiety. *Neuropharmacology 70*, 338−347.

(44) Bymaster, F. P., Dreshfield-Ahmad, L. J., Threlkeld, P. G., Shaw, J. L., Thompson, L., Nelson, D. L., Hemrick-Luecke, S. K., and Wong, D. T. (2001) Comparative affinity of duloxetine and venlafaxine for serotonin and norepinephrine transporters in vitro and in vivo, human serotonin receptor subtypes, and other neuronal receptors. *Neuropsychopharmacology 25*, 871−880.

(45) Wang, J., Morin, P., Wang, W., and Kollman, P. A. (2001) Use of MM-PBSA in reproducing the binding free energies to HIV-1 RT of TIBO derivatives and predicting the binding mode to HIV-1 RT of efavirenz by docking and MM-PBSA. *J. Am. Chem. Soc. 123*, 5221−5230.

(46) Xue, W., Wang, P., Li, B., Li, Y., Xu, X., Yang, F., Yao, X., Chen, Y. Z., Xu, F., and Zhu, F. (2016) Identification of the inhibitory mechanism of FDA approved selective serotonin reuptake inhibitors: an insight from molecular dynamics simulation study. *Phys. Chem. Chem. Phys. 18*, 3260−3271.

(47) Skeby, K. K., Sorensen, J., and Schiott, B. (2013) Identification of a common binding mode for imaging agents to amyloid fibrils from molecular dynamics simulations. *J. Am. Chem. Soc. 135*, 15114−15128.

(48) Barer, M. R., and Harwood, C. R. (1999) Bacterial viability and culturability. *Adv. Microb. Physiol. 41*, 93−137.

(49) Andersen, J., Kristensen, A. S., Bang-Andersen, B., and Stromgaard, K. (2009) Recent advances in the understanding of the

DOI: 10.1021/acschemneuro.7b00490
ACS Chem. Neurosci. 2018, 9, 1128−1140

interaction of antidepressant drugs with serotonin and norepinephrine transporters. *Chem. Commun.*, 3677−3692.
(50) Wang, P., Fu, T., Zhang, X., Yang, F., Zheng, G., Xue, W., Chen, Y., Yao, X., and Zhu, F. (2017) Differentiating physicochemical properties between NDRIs and sNRIs clinically important for the treatment of ADHD. *Biochim. Biophys. Acta, Gen. Subj. 1861*, 2766−2777.
(51) Wang, P., Zhang, X., Fu, T., Li, S., Li, B., Xue, W., Yao, X., Chen, Y., and Zhu, F. (2017) Differentiating Physicochemical Properties between Addictive and Nonaddictive ADHD Drugs Revealed by Molecular Dynamics Simulation Studies. *ACS Chem. Neurosci. 8*, 1416−1428.
(52) Yang, F. Y., Fu, T. T., Zhang, X. Y., Hu, J., Xue, W. W., Zheng, G. X., Li, B., Li, Y. H., Yao, X. J., and Zhu, F. (2017) Comparison of computational model and X-ray crystal structure of human serotonin transporter: potential application for the pharmacology of human monoamine transporters. *Mol. Simul. 43*, 1089−1098.
(53) Li, B., Tang, J., Yang, Q., Li, S., Cui, X., Li, Y., Chen, Y., Xue, W., Li, X., and Zhu, F. (2017) NOREVA: normalization and evaluation of MS-based metabolomics data. *Nucleic Acids Res. 45*, W162−170.
(54) Penmatsa, A., Wang, K. H., and Gouaux, E. (2015) X-ray structures of Drosophila dopamine transporter in complex with nisoxetine and reboxetine. *Nat. Struct. Mol. Biol. 22*, 506−508.
(55) Grouleff, J., Ladefoged, L. K., Koldso, H., and Schiott, B. (2015) Monoamine transporters: insights from molecular dynamics simulations. *Front. Pharmacol. 6*, 235.
(56) Zheng, G., Xue, W., Yang, F., Zhang, Y., Chen, Y., Yao, X., and Zhu, F. (2017) Revealing vilazodone's binding mechanism underlying its partial agonism to the 5-HT1A receptor in the treatment of major depressive disorder. *Phys. Chem. Chem. Phys. 19*, 28885−28896.
(57) Larkin, M. A., Blackshields, G., Brown, N. P., Chenna, R., McGettigan, P. A., McWilliam, H., Valentin, F., Wallace, I. M., Wilm, A., Lopez, R., Thompson, J. D., Gibson, T. J., and Higgins, D. G. (2007) Clustal W and Clustal X version 2.0. *Bioinformatics 23*, 2947−2948.
(58) Arnold, K., Bordoli, L., Kopp, J., and Schwede, T. (2006) The SWISS-MODEL workspace: a web-based environment for protein structure homology modelling. *Bioinformatics 22*, 195−201.
(59) Laskowski, R. A., MacArthur, M. W., Moss, D. S., and Thornton, J. M. (1993) PROCHECK: a program to check the stereochemical quality of protein structures. *J. Appl. Crystallogr. 26*, 283−291.
(60) *PyMOL Molecular Graphics System*. v. 1.3, Schrödinger, LLC.
(61) *Glide*, v. 5.5, Schrödinger, LLC, New York, NY, 2009.
(62) *LigPrep*, v. 2.3, Schrödinger, LLC, New York, NY, 2009.
(63) Kaminski, G. A., Friesner, R. A., Tirado-Rives, J., and Jorgensen, W. L. (2001) Evaluation and Reparametrization of the OPLS-AA Force Field for Proteins via Comparison with Accurate Quantum Chemical Calculations on Peptides. *J. Phys. Chem. B 105*, 6474−6487.
(64) *Epik*, v. 2.0, Schrödinger, LLC, New York, NY, 2009.
(65) *Maestro*, v. 9.0, Schrödinger, LLC, New York, NY, 2009.
(66) Lomize, M. A., Pogozheva, I. D., Joo, H., Mosberg, H. I., and Lomize, A. L. (2012) OPM database and PPM web server: resources for positioning of proteins in membranes. *Nucleic Acids Res. 40*, D370−376.
(67) Wu, E. L., Cheng, X., Jo, S., Rui, H., Song, K. C., Davila-Contreras, E. M., Qi, Y., Lee, J., Monje-Galvan, V., Venable, R. M., Klauda, J. B., and Im, W. (2014) CHARMM-GUI Membrane Builder toward realistic biological membrane simulations. *J. Comput. Chem. 35*, 1997−2004.
(68) Hornak, V., Abel, R., Okur, A., Strockbine, B., Roitberg, A., and Simmerling, C. (2006) Comparison of multiple Amber force fields and development of improved protein backbone parameters. *Proteins: Struct., Funct., Genet. 65*, 712−725.
(69) De Vivo, M., Masetti, M., Bottegoni, G., and Cavalli, A. (2016) Role of Molecular Dynamics and Related Methods in Drug Discovery. *J. Med. Chem. 59*, 4035−4061.
(70) *AMBER*, v 14, University of California, San Francisco, 2014.
(71) Darden, T., York, D., and Pedersen, L. (1993) Particle mesh Ewald: An N·log(N) method for Ewald sums in large systems. *J. Chem. Phys. 98*, 10089−10092.
(72) Springborg, M., and Kirtman, B. (2007) Efficient vector potential method for calculating electronic and nuclear response of infinite periodic systems to finite electric fields. *J. Chem. Phys. 126*, 104107.
(73) Aldeghi, M., Heifetz, A., Bodkin, M. J., Knapp, S., and Biggin, P. C. (2016) Accurate calculation of the absolute free energy of binding for drug molecules. *Chem. Sci. 7*, 207−218.
(74) Sun, H., Li, Y., Shen, M., Tian, S., Xu, L., Pan, P., Guan, Y., and Hou, T. (2014) Assessing the performance of MM/PBSA and MM/GBSA methods. 5. Improved docking performance using high solute dielectric constant MM/GBSA and MM/PBSA rescoring. *Phys. Chem. Chem. Phys. 16*, 22035−22045.
(75) Chen, F., Liu, H., Sun, H., Pan, P., Li, Y., Li, D., and Hou, T. (2016) Assessing the performance of the MM/PBSA and MM/GBSA methods. 6. Capability to predict protein-protein binding free energies and re-rank binding poses generated by protein-protein docking. *Phys. Chem. Chem. Phys. 18*, 22129−22139.
(76) Li, B., Tang, J., Yang, Q., Cui, X., Li, S., Chen, S., Cao, Q., Xue, W., Chen, N., and Zhu, F. (2016) Performance Evaluation and Online Realization of Data-driven Normalization Methods Used in LC/MS based Untargeted Metabolomics Analysis. *Sci. Rep. 6*, 38881.
(77) Sun, H., Li, Y., Tian, S., Xu, L., and Hou, T. (2014) Assessing the performance of MM/PBSA and MM/GBSA methods. 4. Accuracies of MM/PBSA and MM/GBSA methodologies evaluated by various simulation protocols using PDBbind data set. *Phys. Chem. Chem. Phys. 16*, 16719−16729.
(78) Sun, H., Chen, P., Li, D., Li, Y., and Hou, T. (2016) Directly Binding Rather than Induced-Fit Dominated Binding Affinity Difference in (S)- and (R)-Crizotinib Bound MTH1. *J. Chem. Theory Comput. 12*, 851−860.
(79) Wang, Z., Sun, H., Yao, X., Li, D., Xu, L., Li, Y., Tian, S., and Hou, T. (2016) Comprehensive evaluation of ten docking programs on a diverse set of protein-ligand complexes: the prediction accuracy of sampling power and scoring power. *Phys. Chem. Chem. Phys. 18*, 12964−12975.
(80) Tippmann, S. (2015) Programming tools: Adventures with R. *Nature 517*, 109−110.
(81) Letunic, I., and Bork, P. (2007) Interactive Tree Of Life (iTOL): an online tool for phylogenetic tree display and annotation. *Bioinformatics 23*, 127−128.

DOI: 10.1021/acschemneuro.7b00490
ACS Chem. Neurosci. 2018, 9, 1128−1140